International Journal of Advanced Technology and Engineering Exploration, Vol 11(111)
ISSN (Print): 2394-5443 ISSN (Online): 2394-7454
http://dx.doi.org/10.19101/IJATEE.2023.10102196

Research Article

Convolutional neural network based detection of lung adenocarcinoma by amalgamating hybrid features

Manika Jha[1*], Richa Gupta[2] and Rajiv Saxena[3]
Research Scholar, Department of Electronics and Communication Engineering, Jaypee Institute of Information Technology, 201309, Noida, India[1]
Associate Professor, Department of Electronics and Communication Engineering, Jaypee Institute of Information Technology, 201309, Noida, India[2]
Adjuct Professor, Department of Electronics and Communication Engineering, Jaypee Institute of Information Technology, 201309, Noida, India[3]

Received: 28-August-2023; Revised: 07-February-2024; Accepted: 09-February-2024

Abstract
Lung adenocarcinoma is a frequent type of lung cancer among the Asian population and usually develops in individuals with a cigarette smoking history. The mortality risk due to this cancer can only be reduced with reliable early detection methods and screening programs. X-rays and computed tomography (CT) scans are commonly used to identify lung adenocarcinoma manually. However, manual analysis of lung radiographs is typically laborious and error-prone. Thus, an intuitive approach is advantageous. This paper employed a lightweight neural network comprising 2 hidden layers and efficient handcrafted features for the automatic detection of lung adenocarcinoma. A total of 4834 CT scans (2226 normal and 2608 adenocarcinoma infected lung) have been considered for training and testing purposes. The model achieved an accuracy of 100% with a unity value of each specificity, precision, recall, F1-Score, and area under the receiver operating characteristic (AUROC) on the benchmark lung adenocarcinoma dataset extracted from the lung image database consortium image collection (LIDC-IDRI). The suggested method is fast, efficient, and computationally less complex for the considered dataset compared to the current techniques available in the literature. It contributes to the medical community conducting large-scale screening programs.

Keywords
Lung cancer, CADx, Feature extraction, Neural network, LIDC-IDRI.

1.Introduction
Adenocarcinomas typically develop in peripheral lung tissue and account for nearly 40% of lung cancer cases. Adenocarcinoma is prevalent in people who have never smoked, even though smoking is the primary cause of most disease occurrences [1]. Although the pathophysiology of adenocarcinoma is complex, it typically exhibits a histologic progression from cells found in normal lungs to cells that are certainly irregular. A variety of unique molecular and genetic processes influence this evolution. Clinicians usually identify the lesion or tumour through imaging modalities, such as computed tomography (CT) or X-ray, followed by a lung biopsy test, which is vital to confirm the diagnosis [2]. The classification is based on the size of the tumour, the pattern of cell proliferation, and the degree of cell infiltration into healthy lung tissues.

*Author for correspondence

The terms adenocarcinoma in situ, minimally invasive adenocarcinoma and invasive adenocarcinoma describes a step-by-step pathologic progression in the natural course of adenocarcinoma development [3]. The treatment depends on the extent of the spread of the primary tumour. Targeted therapy, radiotherapy, chemotherapy, surgical resection and immunotherapy are performed on patients to remove malignant cells [4]. The architecture of the proposed lung adenocarcinoma detection model is presented in *Figure 1*.

Lung adenocarcinoma is the most prevalent type of lung cancer and is a type of non-small cell lung cancer (NSCLC). Adenocarcinoma develops specifically from the cells that border the tiny air sacs (alveoli) in the lungs and is more commonly observed in the lungs' periphery. It is the most prevalent type of lung cancer and is frequently observed in nonsmokers. Adenocarcinoma is

distinguished by the growth of glandular tissue. Cancer cells seem gland-like under a microscope and may create mucus [5]. This histological subtype differs from NSCLC subtypes squamous cell carcinoma and giant cell carcinoma. While smoking is a major risk factor for lung cancer, particularly adenocarcinoma, it can also occur in nonsmokers. Exposure to passive smoke, environmental contaminants, radon gas, and a family history of lung cancer are all risk factors [6].

Lung adenocarcinoma symptoms include a persistent cough, shortness of breath, chest pain, blood in the cough, exhaustion, weight loss, and recurring respiratory infections. The prognosis for lung adenocarcinoma varies greatly depending on the stage of the disease at the time of diagnosis and other individual circumstances. Early detection improves the odds of successful therapy in general. Individuals at risk, particularly those with a history of smoking or other relevant risk factors, should have regular screenings and seek medical assistance if they encounter any symptoms of lung cancer. Early detection and advancements in treatment choices have resulted in better results for many people with lung adenocarcinoma [7, 8].

In most cases, lung adenocarcinoma enters an advanced stage at the time of diagnosis. According to various reports related to early cancer detection, if lung cancer is identified early enough, over 80% of cases can be cured. The survival rate is only 5% if cancer spreads to sections of the body other than the lungs, compared to 70% if the cancer is identified early. However, the recent increase in screening programs for the early detection of lung cancers worldwide has produced a large volume of image modality data. Visual interpretation of such medical databases is time-consuming and dependent on the individual. This increases the risk of human error and can lead to cancer misinterpretation [9].

Lung cancer necessitates more attention from the medical, biological, and scientific disciplines to develop novel solutions to enhance early diagnosis, which aids in medical decisions and assesses actions to improve health care. A massive amount of CT scan imaging data for the lungs could aid in the detection of lung cancer. These images can be used by machine learning and deep learning (DL) algorithms to improve cancer prediction and detection as early as feasible, as well as to determine the best treatment techniques. Machines can now analyse high-dimensional data such as pictures, multidimensional anatomical scans, and videos thanks to DL approaches. Convolutional neural networks (CNN) and recurrent neural networks (RNN) are common DL models that are frequently used for image and sequential data classification [10].

As a result, an automated system is critical for guiding the radiologist in the appropriate diagnosis of lung adenocarcinoma. Recent advances in image processing and machine learning have resulted in spectacular, cutting-edge advances in radiography. There has been ongoing research on the subject of lung adenocarcinoma diagnosis using machine learning/DL and numerous developments have been made. There are, nevertheless, some significant research gaps and issues that must be overcome. Here are a few instances of potential research gaps:

- Optimising early detection models: More research is needed to develop models that can detect lung cancer at the earliest possible stage when intervention is most successful. This entails detecting small patterns in imaging data that could be symptomatic of early-stage tumours.
- Denoising the imaging data: It is critical to ensure zero noise in imaging data gathered from various sources to construct robust models that generalise effectively.
- Development of a lightweight machine learning model for lung adenocarcinoma detection is essential for practical deployment in resource-constrained environments, such as mobile devices or low-power computing systems.

The proposed work also includes a computer-aided diagnostic model that is lightweight, computationally simple, and highly precise to categorize two-dimensional computed tomography (2D-CT) scans into the classes of normal or adenocarcinoma. Following is a summary of the significant contributions of the proposed model:

A. Dataset of 2226 normal and 2608 adenocarcinoma 2D-CT scans have been extracted from the lung image database consortium image lung image database consortium image collection (LIDC-IDRI) dataset.
B. Initial pre-processing and denoising through a two-dimensional fractional Fourier transform (2D-FrFT) have been done on the training set to enhance the visual interpretation of CT scans.
C. Total of 64 handcrafted features have been extracted from the training set of a dataset through shape-based (8), textural analysis (32) and wavelet transform (24).

D. A 2-layer neural network has been developed to classify normal and adenocarcinoma images.

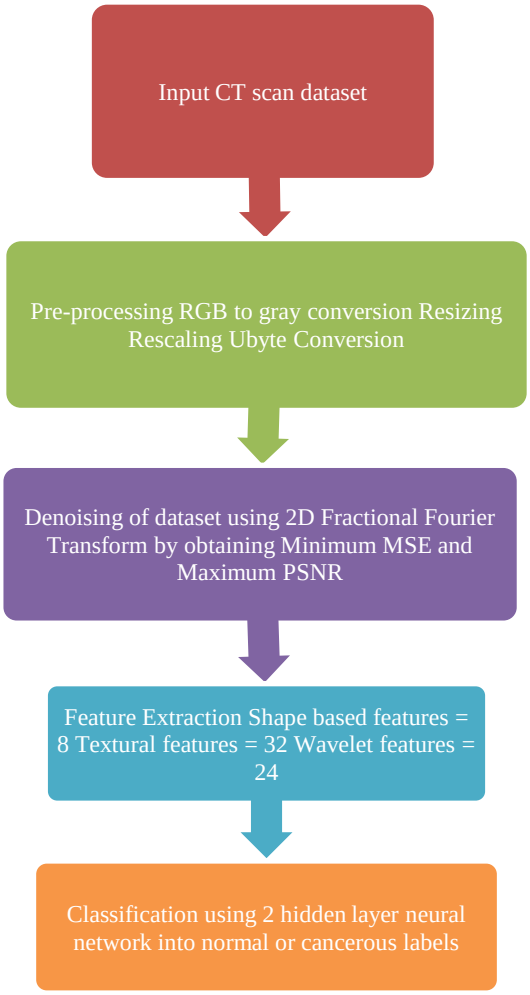

Figure 1 Overall architecture of the proposed lung adenocarcinoma detection model

This paper is structured as follows: Various state-of-the-art literature related to lung cancer have been stated in section 2. A thorough description of the proposed architecture is presented in section 3. The experimental results are shown in section 4. The analysis of simulation results is discussed in section 5. Section 6 concludes with recommendations for future work.

2.Literature review

In recent years, there has been a significant increase in research work related to non-invasive cancer detection. While some try to improve the prediction performance using advanced approaches, others focus on reducing the computational complexity. In addition to that, feature extraction has gained recognition for enhancing accuracy. This section includes a literature survey on lung cancer detection. For better understanding, the research works have been divided into two subsections-Machine-learning based detection and DL-based detection.

2.1Machine learning based methods

Chabat et al. [11] developed a 13-dimensional vector of local texture information that includes statistical moments of a CT scan along with attenuation distribution, acquisition-length parameters, and co-occurrence descriptors. A supervised Bayesian classifier is used for the feature segmentation. Texture aspects of solitary pulmonary nodules (SPNs) discovered by CT scans are assessed by Zhu et al. [12]. After 300 genetic generations, roughly 25 traits were picked out of 67 features. The dimensions of the feature vector are decreased using five scalar metrics - maximum, entropy, energy, contrast, and homogeneity- retrieved from each co-occurrence matrix. At last, a support vector Machine (SVM) based classifier is used for the classification. Kadir and Gleeson [13] reviewed several machine learning approaches developed to date and highlighted their significant strengths and limitations. The paper discussed various challenges in validating such techniques for adopting them in clinical usage. Makaju et al. [14] used watershed segmentation to segment the input image. The image with cancer nodules is identified in the segmentation results. After that, features for the segmented cancer nodules were recovered utilizing area, perimeter, eccentricity, centroid, diameter, and pixel mean intensity. Finally, an SVM was used to classify cancer nodules.

Dev et al. [15] provided a computer-aided categorization approach for CT scans of the lungs. The proposed method has been put into practice using MATLAB. The many phases include acquiring input data, pre-processing, segmentation, feature extraction, and classification through SVM. This model has attained an overall accuracy of 86.25%. Hussain et al. [16] used machine learning algorithms such as naïve Bayes, SVM, polynomial kernels and decision trees to classify lung cancer images. They have also employed reconstruction component analysis and autoencoder to extract morphological and textural features. They attained an area under curve (AUC) of 1.00, providing a good potential for diagnostic applications. To effectively identify lung and colon cancer, Talukder et al. [17] presented a hybrid feature extraction approach. For several histological lung and colon datasets, an integration of

deep feature extraction and a machine learning classifier has been employed.

2.2Deep-learning based methods

Automated analytic techniques have been now in high demand in the pathology sector since they can significantly lessen the load, accelerate diagnosis, and enable timely cure. CNNs have delivered incredible progress in several areas of medical diagnostics through signal and image processing [18]. Razmjooy et al. [19] developed a system through multiscale sample entropy (MSE), multiscale fuzzy entropy (MFE), refined composite multiscale fuzzy entropy (RCMFE), and multiscale permutation entropy (MPE) features extracted using mean and tree approach. MFE-based texture features provided the highest accuracy. In the dynamic analysis of lung cancer, experimental outcomes showed that the developed model with RCMFE features outperformed other existing models.

Lakshmanaprabu et al. [20] presented an automatic lung cancer screening system based on CT scans of the lungs. To assess the images, they combined an optimal deep neural network (DNN) with linear discriminate analysis (LDA). Wang et al. [21] proposed a lightly supervised technique for diagnosing lung cancer from radiographs that is both efficient and quick. First, they used a fully convolutional network (FCN) based on patches to extract illustrative deep features while saving the discriminative parts. Subsequently, with multiple feature combinations and block selection strategies, a global holistic description has been produced. It was then loaded into a random forest classifier for classification. A neural ensemble-based detection (NED) method was proposed by Zhou et al. [22]. The model used an ensemble approach, built through a neural network of combinational layers to identify cells related to lung cancer. This approach has been found to be highly accurate in identifying cancer cells. Another method for diagnosing lung cancer was proposed by Shakeel et al. [23]. Noise was removed from the input images using weighted mean histogram equalization, and image quality was improved using the advanced version of profuse clustering.

DL has been applied to predict lung cancer using spectral information derived from the region of interest. Aggarwal et al. [24] built a computer aided diagnostic (CAD) system that could predict lung cancer using CT and position emission tomography (PET) images. In order to enhance the lung cancer prediction process, the research work investigates various methodologies, including image segmentation and nodule detection. The dataset has been split into training and testing images for the analysis, which evaluated the performance of the CAD system. *Table 1* presents a few more recent lung cancer detection research papers with their results and limitations.

Table 1 Recent models associated with lung adenocarcinoma detection

Author (Year)	Method	Categorical accuracy (%)	Advantages	Limitations
Deepa and Suganthi (2020) [25]	Contourlet and Kernel-induced random forest	94.00	Fuzzy space representation, Implemented on various datasets for generality	Complex system, Lower accuracy
Hoque et al. (2020) [26]	Contrast stretching and SVM	96.15	Effective image enhancement and feature extraction techniques	Limited dataset, Lower accuracy
Mathews and Jeyakumar (2020) [27]	Anisotropic diffusion filtering and CNN	97.60	Unsharp masking enhancement, Super pixel segmentation based iterative clustering	Lack of integration with fuzzy genetic optimization techniques
Ozdemir et al. (2019) [28]	Three-dimensional CNN	94.00	Improved diagnostic precision and fewer false positives	Restricted by computing power and labelled data accessibility
Ali et al. (2020) [29]	Texture CNN	96.69	Extremely sensitive and specific	Large volumes of training data are required
Kareem et al. (2021) [30]	SVM	89.88	Lightweight model with lower parameters	Lower accuracy, small sample size
Sori et al. (2021) [31]	Residual learning denoising model (DR-Net)	87.80	Efficient denoising, Joint integration of local and global features	Large volumes of training data are required

Author (Year)	Method	Categorical accuracy (%)	Advantages	Limitations
Priya et al. (2021) [32]	Deep Belief Network	96.60	Dimension reduction, good classification accuracy for pulmonary images.	Large datasets and specialized knowledge are required
Neal et al. (2021) [33]	Three dimensional CNN	97.71	Lightweight architecture, superior classification accuracy than existing methods	Restricted by computing power
Asuntha and Srinivasan (2021) [34]	Fuzzy particle swarm optimization (FPSO)+CNN	95.62	Efficient feature extraction techniques	High false positive rate
Ramana and Kumar (2022) [35]	Capsule Networks and Transfer Learning	98.50	High accuracy, Lower pre-processing time	Complex model with high trainable parameters
Causey et al. (2022) [36]	CNN	92.00	Reduced false positive rate	Lower AUC and longer interpretation time
Kumar et al. (2023) [37]	DL	93.40	Improved diagnostic precision and fewer false positives	Huge volumes of training data required
Tiwari et al. [38]	Hybrid Neural Network	99.45	high accuracy rate of 99.45% and reduced false positives	Longer training time

The discussed research works mainly project a shift of biomedical experts from simple classification models to extensive feature extraction techniques. Newer and more efficient features could provide more critical information about malignant tumors, than a 100-layer DNN. Also, the accuracy, false positive rate and computational complexity of these available models are not satisfactory for developing a computer-aided diagnostic system deployed either on a mobile application or website. The proposed model improves accuracy by employing effective denoising and feature extraction techniques to obtain all critical information from lung adenocarcinoma 2D-CT scans. A lightweight neural network classifies the normal and lung adenocarcinoma scans with reduced computational complexity and fewer parameters.

3.Methods

This section includes details about the dataset, pre-processing techniques, denoising algorithm and classification through a neural network.

3.1Dataset description

The LIDC-IDRI dataset provided 4834 thoracic 2D-CT scans with marked lesion annotations. It is a global resource that is available online for the development, training, and assessment of CAD methods for lung cancer detection and diagnosis [39]. The original radiologists of this dataset individually reviewed each 2D-CT scan and labelled lesions as "nodule > or =3 mm," "nodule 3 mm," or "non-nodule > or =3 mm" in one of three categories during the blinded-read phase. The proposed classification model has been developed using 2226 normal and 2608 adenocarcinoma-infected 2D-CT scans of the lungs.

3.2Pre-processing of the training set

Pre-processing enhances the quality of images by removing undesirable distortions or increasing important visual properties required for consequent analysis [40]. The following are the steps taken into consideration to pre-process the LIDC-IDRI training set.

Step 1: To reduce computational complexity, the dataset is first pre-processed with RGB to gray conversion. Equation 1 below, provides the gray values required to transfer RGB values of a pixel.

$$gray=0.2125\ R+0.7154\ G+0.0721\ B \quad (1)$$

Step 2: Resizing the dataset image size to 512×512 pixels. The new image size is obtained by using numpy.resize() function. It includes the repeated copies of pixel values present in the initial image.

Step 3: The dataset is then rescaled from 0 to 1 using Min-max normalization.

Step 4: At last, ubyte conversion is done to convert all images to unsigned byte format, with values in the range 0 to 255.

3.3Denoising of training set of the dataset

The most complex part of medical modalities is to obtain an image without any information loss. The random variation of the original pixel value is known as noise. Noise degrades image quality, which is

especially noticeable when the objects being photographed are small and have low contrast. The images obtained during the collection and/or subsequent processing phases are likely to be corrupted by different types of noises. The removal of disruptions is extremely important since medical images have poor contrast compared to images taken under normal lighting, which makes it more difficult to identify diseases. Thus, denoising medical images is an essential pre-processing phase for medical imaging systems [41, 42].

CT scan employs ionizing radiation, and the dose of radiation is cumulative. Low dose computed tomography (LDCT) is thus used to reduce the effects of ionizing radiation. A lower radiation dose results in an inferior image. For instance, for every factor of √2 drop in radiation, the noise increases by a factor of 2.

Furthermore, for accurate diagnosis, the ratio between significant tissue contrasts and noise amplitude must be large enough. As a result, the radiation dose cannot be easily lowered. This is one of the most significant obstacles to use LDCT scans for disease diagnosis [43, 44].

To overcome this problem, several modified filters such as mean, median, wiener, wavelet, gaussian, median, fourier transform are introduced. These filters improve the quality of 2D-CT scans to some extend but stills lack a satisfactory level of metrics. After implementing all the above-discussed filters, 2D-FrFT has been applied to the dataset to reduce artifacts and obtain a noise-free dataset for further experimentation. 2D-FrFT performed better than the other filters in terms of mean square error (MSE) and peak signal to noise ratio (PSNR) [45, 46].

2D-FrFT transform is a set of complex exponentials with varying magnitudes, frequencies, and phases in a fractional domain that represents an image [47]. The FrFT of the signal f(t) is mathematically represented in Equation 2 for one-dimensional FrFT:

$$T_F^{\varphi}[f(t)] = F^{\varphi}(u_{\varphi}) = \int_{-\infty}^{\infty} f(t) K_{\varphi}(t, u_{\varphi}) dt, \quad (2)$$

where,

$$K_{\varphi}(t, u_{\varphi}) = \frac{1}{2\pi}\sqrt{1 - jcot\varphi}\, exp\left[\frac{j}{2}\left(t^2 + u_{\varphi}^2\right)cot\varphi - jtu_{\varphi}csc\varphi\right] \quad (3)$$

K_{φ} is the kernel of FrFT. T_F^{φ} and φ represents the operator and rotational angle, respectively. The inverse of the obtained signal can be obtained through a backward rotation angle '$-\varphi$', shown in Equation 4:

$$f(t) = \int_{-\infty}^{\infty} K_{-\varphi}(t, u_{\varphi}) F^{\varphi}(u_{\varphi}) du_{\varphi} \quad (4)$$

By individually repeating the transform in the x and y directions and considering a different kernel, the FrFT expression can be effectively converted to two dimensions. The separable 2D-FrFT of orders φ $(x - axis)$ and γ $(y - axis)$ is shown in Equation 5:

$$T_F^{\varphi,\gamma}[f(x,y)] = F^{\varphi,\gamma}(u_{\varphi}, v_{\gamma}) = \iint_{-\infty}^{\infty} f(x,y) K_{\varphi,\gamma}(x, y, u_{\varphi}, v_{\gamma}) dx dy, \quad (5)$$

where,

$$K_{\varphi,\gamma}(x, y, u_{\varphi}, v_{\gamma}) = K_{\varphi}(x, u_{\varphi}) v_{\gamma}) K_{\varphi}(y, v_{\gamma})$$

$$= \frac{1}{2\pi}\sqrt{1 - jcot\varphi}\sqrt{1 - jcot\gamma}\, exp\left[\frac{j}{2}\left(x^2 + u_{\varphi}^2\right)cot\varphi - jxu_{\varphi}csc\varphi\right] exp\left[\frac{j}{2}\left(y^2 + v_{\gamma}^2\right)cot\gamma - jyv_{\gamma}csc\gamma\right] \quad (6)$$

The f (x, y) signal can be retrieved back by implementing 2D-FrFT operation by backward angles $(-\varphi, -\gamma)$ as:

$$f(x,y) = \int_{-\infty}^{\infty}\int_{-\infty}^{\infty} F^{\varphi,\gamma}(u_{\varphi}, v_{\gamma})\, K_{-\varphi,-\gamma}(u_{\varphi,} v_{\gamma}, x, y) du_{\varphi} dv_{\gamma} \quad (7)$$

Now, for an M × N matrix, the 2D discrete FrFT can be computed through Equation 8:

$$F^{\varphi,\gamma}(u_{\varphi}, v_{\gamma}) = \sum_{x=0}^{M-1}\sum_{y=0}^{N-1} f(x,y)\, exp\left[\frac{j}{2}\left(x^2 + u_{\varphi}^2\right)cot\varphi - jxu_{\varphi}csc\varphi\right] exp\left[\frac{j}{2}\left(y^2 + v_{\gamma}^2\right)cot\gamma - jyv_{\gamma}csc\gamma\right] \quad (8)$$

The 2D-FrFT is a comprehensive transformation of the traditional fourier transform with fractional parameters φ and γ, along with operator a, related as φ = γ = aπ/2. The FrFT operator 'a' has values ranging from 0 to 1. The presence of noise in the signal or image to be processed using 2D-FrFT is controlled by manipulating the value of the fractional operator [48].

The proposed denoising approach is a five-stage process, described below:

Stage 1: For evaluating the performance of the 2D-FrFT based algorithm, images are artificially corrupted with Python generated additive random noise of mean 0 and variance 0.05.

Stage 2: For obtaining the optimum value of the FrFT operator, a set of 20 random images are

considered from the noisy dataset and filtered with varying values of 'a' from 0 to 1.

Stage 3: By investigating the results of one such set recorded in *Table 2*, it is evident that at a = 0.7, images get the minimum value of RMSE.

Stage 4: The 2D-FrFT filter with a = 0.7 is then applied to the noisy dataset, and the fractional fourier time-frequency domain spectrum removes all high-frequency noisy components.

Stage 5: Finally, inverse FrFT is used for proper reform of the denoised image back to the time domain.

Stage 6: Other filters such as mean, median, wiener, wavelet, gaussian, median, fourier transform are also employed to denoise the original dataset. The average values of MSE and PSNR have been calculated and presented in *Table 3*. The qualitative aspect of all filters utilized for the noise removal is shown in *Figure 2.*

Table 2 Analysis of randomly selected 20 images from corrupted LIDC-IDRI Dataset by minimum mean square error (MMSE) at various levels of fractional Fourier operator (a)

Images	Values of fractional operator (a)										
	0	**0.1**	**0.2**	**0.3**	**0.4**	**0.5**	**0.6**	**0.7**	**0.8**	**0.9**	**1**
Image 1	1.938	1.0983	1.9722	1.2087	0.8622	0.7357	0.1973	0.0928	0.7386	1.2512	2.9831
Image 2	2.0993	1.8263	2.873	1.0892	0.9738	0.9833	0.1889	0.0728	0.9027	1.9793	3.9734
Image 3	1.6357	1.0821	1.8723	1.3082	0.8267	0.8278	0.7872	0.2978	0.6728	1.0833	1.9733
Image 4	0.9837	0.9372	1.4973	1.2089	1.0833	0.7563	0.0768	0.0043	0.9378	1.0838	1.0973
Image 5	0.8368	1.0873	1.7373	1.1839	1.0377	0.6356	0.0927	0.8272	0.8839	0.8297	1.8733
Image 6	1.7363	1.8963	1.4082	1.0929	2.983	0.3978	0.5378	0.1236	0.9738	0.9722	2.8642
Image 7	1.9473	1.8735	1.2974	0.9278	1.0839	0.8733	0.8367	0.5738	0.3578	0.9838	2.097
Image 8	1.8646	1.9862	0.9838	0.9278	0.8728	0.9839	0.5467	0.0378	0.7836	0.9882	3.0112
Image 9	2.6468	1.0833	0.9882	1.9303	1.0388	1.0927	0.6484	0.0987	0.7638	1.3974	1.9722
Image10	2.0981	1.9377	1.3974	1.9378	1.9829	0.9278	0.2457	**0.2097**	0.6783	0.9728	2.873
Image 11	1.0838	2.983	0.9728	1.8263	0.9272	0.5682	0.8488	**0.4323**	0.7563	1.0839	1.8723
Image 12	1.0837	1.0839	0.8278	1.0821	0.8633	0.6289	0.4867	**0.3927**	0.6356	0.8728	2.0981
Image 13	1.9378	0.8728	0.7978	0.9372	0.8266	0.7827	0.3864	**0.0229**	0.3978	2.0388	2.0092
Image 14	2.1098	2.0388	1.9379	1.0873	0.7386	0.9982	0.3464	**0.1973**	0.8733	0.9829	1.2087
Image 15	2.8763	1.9829	1.4982	1.8963	0.9027	0.8927	0.7357	**0.1889**	0.9839	1.9272	2.9734
Image 16	0.9738	1.9272	1.0599	1.8735	0.6728	0.9678	0.8467	**0.2872**	0.5638	1.0972	0.9863
Image 17	1.9373	0.2972	1.8272	1.9793	0.9378	0.7788	0.5647	**0.0768**	0.6378	1.7891	1.0833
Image 18	0.9876	0.8917	1.1236	1.0833	0.8839	0.6747	0.3467	**0.0927**	0.9738	1.0973	2.8743
Image 19	1.0937	1.9028	1.5738	1.0838	0.9738	0.9784	0.4739	**0.1082**	0.7367	0.9826	2.0991
Image 20	0.8363	1.5627	0.9378	0.9878	0.8267	0.8494	**0.3567**	0.3873	0.4678	0.9982	1.9829

**Bold indicates the minimum MSE value for individual images.*

Table 3 Comparison of various denoising filters to remove noise present in the corrupted LIDC-IDRI dataset

Parameters	**Mean**	**Median**	**Gaussian**	**Weiner**	**Wavelet**	**Fourier transform – low pass**	**Fourier transform – high pass**	**2D-FrFT with a = 0.7**
Average MSE	9.2408	8.6468	1.9087	1.4091	1.2738	0.8872	10.7588	**0.2765**
Average PSNR	28.8217	37.9795	39.1766	38.911	58.2781	54.3344	50.8768	**63.2356**

Parameters	Mean	Median	Gaussian	Weiner	Wavelet	Fourier transform – low pass	Fourier transform – high pass	2D-FrFT with a = 0.7
Average SSIM	0.9686	0.9786	0.9762	0.9738	0.9881	0.9802	0.9275	**0.9987**

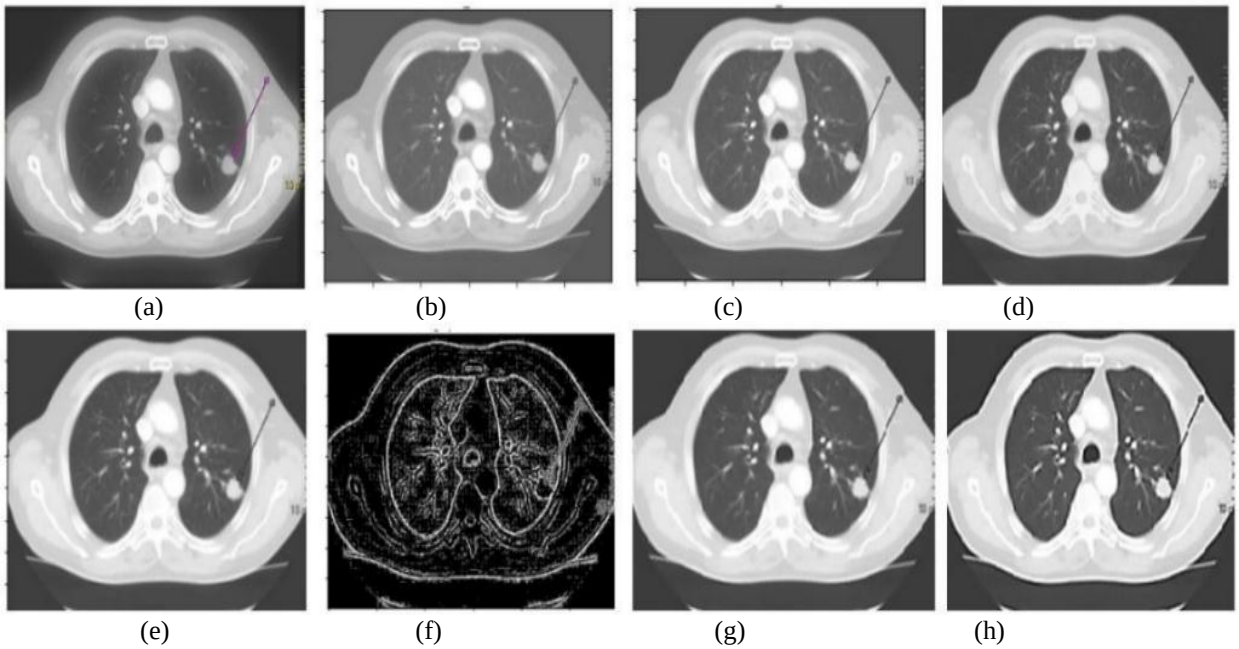

Figure 2 Qualitative Aspect of various denoising filters on a Lung adenocarcinoma 2D-CT scan (a) Original image (b) Mean filter (c) Median (d) Gaussian (e) Weiner (f) Fourier high pass (g) Wavelet (h) 2D-FrFT

3.4Denoising of training set of the dataset

All critical features extracted from the training set to build the proposed model are discussed in following sections.

3.4.1Shape-based features

Shape-related features extract information about the general contour and morphological changes present in any image. They are obtained by implementing contour tracing on binary images. These binary images are attained by thresholding the gray images. The four basic features extracted in this subsection are Tumour length, Tumor width, Tumour area and Aspect ratio [49]. The brief details about these features along with their mathematical expression are illustrated below.

1) Tumour length – It is determined utilizing the stretched extension from the tumour apex to its base. It is denoted by T_l.
2) Tumour width – It is considered by taking a line perpendicular to the axis length which relates to the longest distance. It is denoted by T_w. The relation between T_l and T_w is shown in *Figure 3*.
3) Tumour area – It is a critical variable that can be utilized to classify a tumour type is the overall area covered by it. A reference point, such as the centre of gravity (CG), must be chosen to compute the tumour area. The overall tumour area is computed by aggregating small areas generated by spots. Any two successive sites on the segmented region's borders (where the tumour changes direction) and the reference point are chosen as the three spots. If the two subsequent points revolve around the CG in a clockwise orientation, the areas of these triangles are assigned a positive sign; otherwise, they are assigned a negative value.
4) Aspect ratio – It is the ratio of the tumor's length to its width. The formula to calculate it is T_l/T_w.

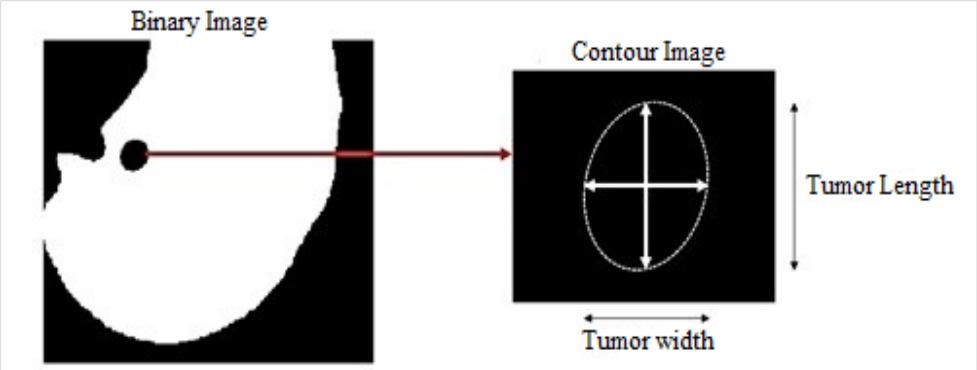

Figure 3 Relationship between tumor length and width

3.4.2Textural features

Texture is an important aspect of human vision that is utilized in many computer vision systems. It is defined as a measure of coarseness, contrast, directionality, line-likeness, regularity, and roughness in many research reports. The textural aspects can be alternatively interpreted as a resemblance of image grouping or as naturalistic environments with semi-repetitive pixel layouts.

The grey level co-occurrence matrix (GLCM) technique, also known as the spatial grey level dependence matrix (SGLDM), considers second-order statistics and pairings of pixels in specific spatial associations. It observes the relationship amid pixels and expresses how often a combination of pixels exists in an image with distance (d) and a specified direction [50, 51]. In the proposed work, 8 textural features – Mean, variance, standard deviation, skewness, kurtosis, energy, entropy, and correlation have been obtained from GLCM.

3.4.3Wavelet features

Wavelet features demonstrate their ability to capture localized spatial frequency information as well as multiresolution properties. The wavelet signal is passed through a series of low and high pass filters, before being transformed into transform coefficients. In the frequency domain, a transformation through a 2 dimensional wavelet permits localization. Dilation and translation of a mother wavelet ψ, shown in Equation 9, yield 1D (child) wavelets:

$$\psi_{j,k}(t) = \frac{1}{\sqrt{2^j}}\psi\left(\frac{t-k2^j}{2^j}\right) \quad (9)$$

where j and k are the scale and shift parameters, respectively. A decomposition is employed, resulting in different frequency bands. The regions of interest are dissected to four levels using a 2-D symlets wavelet. Finally, features are obtained by evaluating the mean, standard deviation, and variance of wavelet coefficients.

3.4.4Fusion of handcrafted features

For the training of the classification model, the shape-based, texture-based, and wavelet-based features, are concatenated together to obtain a feature pool. 8 shape-based features, 32 textural features using GLCM and 24 wavelet features are extracted in this work. The shape-based features have been taken for both lungs, GLCM features are calculated for 4 directions, and wavelet features are obtained for all 8 sub-bands. Finally, a total of 64 features are extracted.

3.5Classification model through neural network

The primary objective of a neural network is to establish a relation between the features present in a dataset. It is constructed using a series of mathematical procedures that replicate the operations of the human brain. A "neuron" is a unit of a neural network that gathers and classifies data using a predetermined structure. Neural networks use weights between decision nodes to reflect the connections, like biological neurons. Inhibitory connections have a negative weight, whereas excitatory links have a positive weight. All inputs are given a weight before being added together. This procedure is known as linear combination. Finally, the amplitude of the output is controlled by its activation function. An acceptable output range, for instance, is often between 0 and 1, though it may also be between -1 and 1. Medical image classification includes identifying and labelling medical images from a predetermined set. The process entails extracting features from an image and assigning labels based on the features extracted [52]. In the proposed work, a neural network with two hidden layers of 128 and 16 neurons, to classify 2D-CT scans into two categories normal and lung adenocarcinoma. The architecture of the proposed

model is shown in *Figure 4*. The splitting of training and testing data is a strategy for evaluating the performance of supervised machine learning algorithms with inputs and target output labels. The training set instructs the model to recognize patterns present in the input dataset by reducing errors between desired outputs and model predictions. To achieve better performance of the proposed neural network, the hyperparameters must be optimized. GridSearchCV is a function provided by the scikit-learn library in Python for performing hyperparameter tuning through an exhaustive search over a specified parameter grid. It is a part of scikit-learn's model selection module and is widely used for finding the best hyperparameter values for a machine-learning model [53]. A brief description of major hyperparameters chosen through GridSearchCV for the lung adenocarcinoma detection model has been provided below:

Adam Optimizer: To optimize weights and minimize the categorical cross-entropy loss function, Adam optimizer has been used. Adam (Adaptive Moment Estimation) incorporates ideas from two previous optimisation algorithms: RMSprop (Root Mean Square Propagation) and Momentum. For each parameter, it keeps two moving averages: the first moment (mean) and the second moment (uncentered variance). These moving averages are used to change the learning rates adaptively during training.

Maximum number of Epochs: The term "maximum epochs" refers to the number of times an entire dataset is transmitted forward and backwards through a neural network during training. For the proposed model MaxEpochs has been set to 200.

Batch Size: The batch size defines the number of samples used in each iteration of training of the model. During the training process, the dataset is divided into batches, and the model's parameters are updated based on the error calculated on each batch. A batch size of 2 has been considered for the proposed model.

Learning Rate: The learning rate has been set to 0.001. It is a scalar that multiplies the gradient of the loss concerning the model parameters. It controls the step size in the parameter space during optimization.

Sigmoid Loss Function: The sigmoid activation is applied to the output layer for binary classification problems, where the goal is to predict either class 0 or class 1.

Dropout Value: The dropout technique involves randomly dropping out (setting to zero) a fraction of the units/neurons in a layer during training. This helps to prevent complex co-adaptations on training data, which can lead to overfitting. The value of dropout has been set to 0.2 for the proposed model.

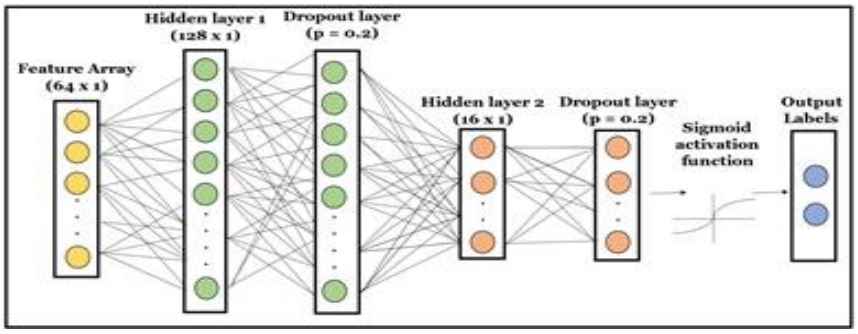

Figure 4 Neural network classifier model with 2 hidden layers

4.Experimental results

The proposed model has been implemented on the platform of Python-Jupyter software (version 3.8) with configurations of Intel(R) Xeon (R) CPU @ 3.30 GHz 8 GB RAM x-64 based processor.

4.1Classifier evaluation – with and without denoising

Pre-processing of 4834 Lung adenocarcinoma images of the LIDC-IDRI dataset has been done through resizing, normalizing, adaptive histogram, ubyte conversion. The images were then denoised using the Fractional Fourier transform filter after comparing it with other conventional filters. After pre-processing, denoising, feature extraction and classification were implemented with three different train-test splits i.e. 70:30, 75:25 and 80:20.

To design a neural network classifier, 2D-CT scans have been grouped into two target classes, containing 2226 normal and 2608 adenocarcinoma. The network

includes two hidden layers and one output classifier layer, trained to classify 2D-CT scan images into target classes. The classification results showed the best performance with an 80:20 train-test split. A total of 3867 training and 967 testing samples were considered to obtain the outcomes. The confusion matrices (with and without FrFT filtering) for the test set of datasets are shown in *Figure 5*. The loss curve shown in *Figure 6*, revealed a decent fit between the training-testing curves and indicates the absence of overfitting or underfitting. To further assess the model's performance, an area under receiver operating characteristic (AUROC) curve has been plotted, as shown in *Figure 7*. The suggested model achieved 100 percent accuracy, sensitivity, and precision in classifying normal images from adenocarcinoma. *Table 4* represents the evaluation metrics with and without filtering the LIDC-IDRI dataset. The matrices indicate the significance of filtering the LIDC-IDRI dataset with 2D-FrFT in reducing the false positive/negative predictions. All the predictions were truly classified in their actual class. The matrix obtained without filtering includes 44 misclassified predictions. Zero false negatives in the proposed model ensure that potentially harmful conditions are not overlooked. Minimizing false negatives in medical diagnostics is of utmost significance as it directly impacts patient outcomes and healthcare effectiveness. The AUROC for both LIDC-IDRI datasets attained a value of 1.00 when the CT scans were filtered by 2D-FrFT. This indicates that the model possesses the ability to accurately discriminate between individuals diagnosed with lung adenocarcinoma and those without the condition.

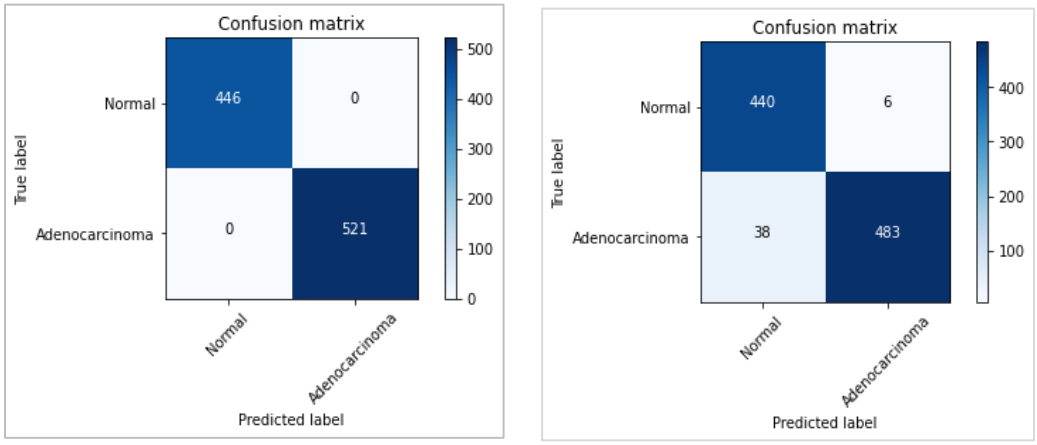

(a) (b)

Figure 5 Confusion matrix of 2D-CT scans classified as – Normal and Adenocarcinoma from the raw LIDC-IDRI dataset, (a) with FrFT filtering (b) without FrFT filtering

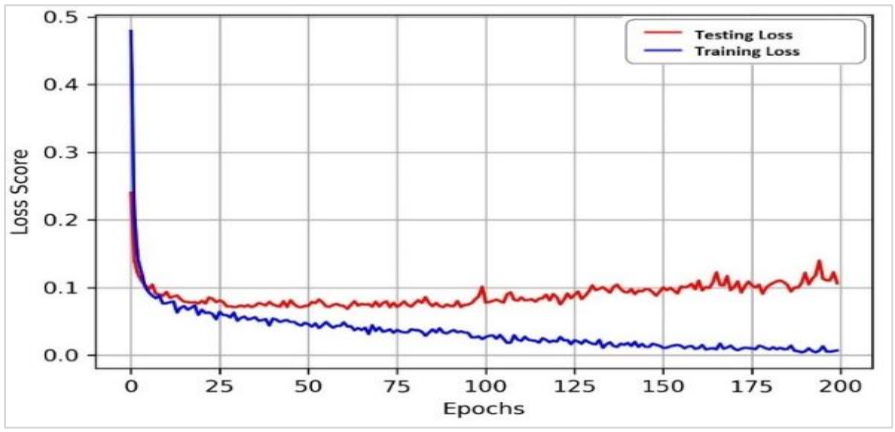

Figure 6 Loss score graph for the training and testing sets

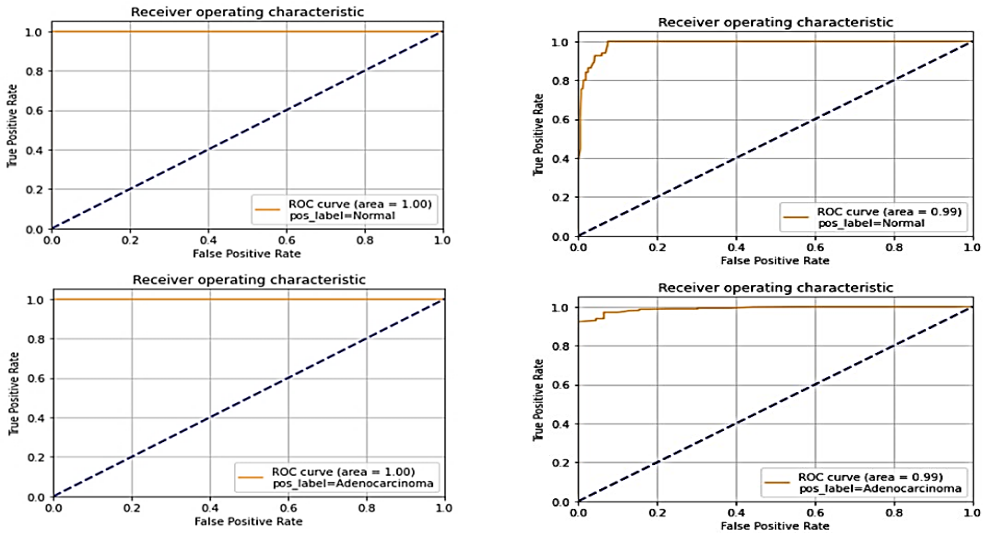

(a) (b)

Figure 7 Receiver operating characteristic (ROC) Curves of classes – normal and adenocarcinoma from the raw LIDC-IDRI dataset, (a) with FrFT filtering (b) without FrFT filtering

Table 4 Performance Evaluation of the classified 2D-CT scans into classes – Normal and Adenocarcinoma, with and without FrFT filtering

		Accuracy (%)	Precision (%)	Sensitivity (%)	F1-Score (%)	AUC
Raw 2D-CT scans	Without FrFT Filtering	95.72	98.77	94.52	96.59	0.99
	With FrFT Filtering	100	100	100	100	1

4.2Analysis of performance metrics for the classification at varying levels of 2d-FrFT operator (a)

A time-frequency distribution is rotated using the fractional Fourier transform. According to this transform, if a = 0, the fractional Fourier transform will result in no change, however, if a = 1, the fractional Fourier transform transforms into a conventional Fourier transform, which rotates the time-frequency distribution by $\pi/2$. The fractional Fourier transform rotates the time-frequency distribution in accordance with for different values of a fractional operator. The results of the fractional Fourier transform for various values of a are depicted in *Table 5*.

Table 5 Values of performance metrics with varying values of fractional operator (a)

Value of (a)	Accuracy (%)	Precision (%)	Sensitivity (%)	F1-Score (%)	AUC
0	95.72	98.77	94.52	96.59	0.99
0.2	95.90	97.38	95.64	96.89	0.99
0.7	100	100	100	100	1
0.9	98.21	98.92	97.29	98.20	0.98
1	97.36	97.40	96.62	97.01	0.98

4.3Comparison of proposed model pre-trained and existing DNN models

The proposed model has also been compared with two recent existing models to detect lung tumors using the LIDC-IDRI dataset. All these existing architectures were implemented in different simulation environments to validate the robustness and pre-eminence of the proposed work. *Table 6* presents the comparison of the proposed classification model with present methods on raw LIDC-IDRI database using evaluation metrics, namely accuracy, sensitivity, false positive rate, AUROC and number of trainable parameters.

Table 6 Comparison of proposed classification model with available state-of-the-art methods

Study	Method	Dataset	Classes	Accuracy (%)	Sensitivity (%)	False positives rate	AUROC	No. of Parameters
VGG16 [37]	-	LIDC-IDRI	Cancerous & Normal	90.1	91.5	0.55	0.90	138.4 million
ResNet-50 [38]	-	LIDC-IDRI	Cancerous & Normal	93.2	93	0.52	0.95	25.6 million
GoogleNet-V1 [39]	-	LIDC-IDRI	Cancerous & Normal	95.2	94.87	0.41	0.95	6.7 million
Asuntha and Srinivasan [34]	FPSO+CNN	LIDC-IDRI	Cancerous & Normal	95.62	97.93	0.38	0.95	≈ 190,000
Masood et.al. [53]	Region proposal network (mRPN) & three-dimensional deep convolutional neural network (3DDCNN)	LIDC-IDRI	Cancerous & Normal	98.51	98.40	0.21	0.96	138.4 million
Proposed	**FrFT+CNN**	**LIDC-IDRI**	**Cancerous & Normal**	**100**	**100**	**0**	**1**	**8450**

5.Discussion

An effective neural network classifier that effectively identified Lung adenocarcinoma 2D-CT scan images from normal patients has been developed in this study. CT scan is a common screening method for detecting lung illnesses and malignancies among many imaging modalities. However, the scans show certain suspicious lung infection lumps, which could lead to a misdiagnosis. As a result, a new method for the categorization of lung adenocarcinoma is vital. The paper demonstrates that this may be done with relatively simple features and a lightweight classifier.

5.1Key findings

The following are the distinguishing features of the proposed strategy:

First, systematic pre-processing of the LIDC-IDRI dataset comprising 4834 2D-CT scan images has been done to resize, normalize and convert them into ubyte format, which results in uniformity and reduced inconsistencies. 2D Fractional Fourier transform has been applied to the images to remove all time-frequency dependent noise in the fractional domain. The filter provides efficient denoising results when compared to the classical median, gaussian, low and high pass filters. Filtering of the dataset with the optimum value of FrFT operator (0.7) has been employed, which resulted in the MMSE and maximum PSNR for all images. The denoised dataset is then gathered for the feature extraction phase.

Second, by generating critical synthetic features and eliminating less significant aspects, ideal features of 2D-CT scan images can be identified, which reduces the overall feature space of models. These artificial features deliver better classification results while reducing the size of the models. Importantly, a more reliable classifier can be created by reducing the ratio between the amount of image features and the number of training data sets per class. Contrary to many earlier machine learning models that examined only the texture-based features in the spatial domain, features from both the spatial domain and frequency domain (Wavelet) have been focused on in the feature extraction step.

Third, a simple neural network comprising two hidden layers has been proposed to detect Lung adenocarcinoma with high accuracy and sensitivity. The findings suggest that by utilizing the proposed classification framework, it is possible to distinguish between Lung adenocarcinoma and normal patients with high accuracy. The suggested framework was shown to have a maximum classification accuracy of 100%, indicating its clinical use in classifying patients using a 2D-CT scan dataset.

5.2Comparison with existing models

The comparison of the systems revealed that the suggested model outperformed the other methods significantly. The most important note is that the proposed model has only ~8,000 parameters, which is much less than common image classification models such as VGG-16, which has 138 million17, GoogleNet-V1, which has 5 million18, and ResNet-50, which has 25 million. To obtain the optimal features, Asuntha and Srinivasan [34] employed feature extraction techniques such as histogram of gradient (HOG), local binary pattern (LBP) and Zernike moment, and then optimized them using FPSO. These characteristics were employed in a DL model to classify lung nodules. The accuracy and sensitivity of this model, FPSO-CNN, were 95.62 per cent and 97.93 per cent, respectively. Masood et al. [53] created a lung nodule identification system based on a 3DDCNN and a multi-region proposal network. 3DDCNN achieves sensitivity, specificity, AUROC, and accuracy of 98.4 percent, 92 percent, 96 percent, and 98.51 percent, respectively, with 2.1 frames per scan. These observations indicate that the proposed system can be a reliable tool that facilitates automatic analysis to assist in the diagnosis of lung adenocarcinoma.

5.3Limitations

The LIDC-IDRI dataset has been extensively used for training lung cancer classification or prediction models, but it comprises limited samples of specifically adenocarcinoma or other NSCLC. Thus, it is challenging to test the model for the unseen data. Also, lung adenocarcinoma can manifest differently among individuals. If the model does not account for this heterogeneity, its predictions may not be accurate for all patients. It's essential to address these limitations through rigorous evaluation, continuous improvement, and collaboration between machine learning experts, clinicians, and domain experts in the field of lung adenocarcinoma. A few interpretability tools or techniques must be used to understand the model's decision-making process.

A complete list of abbreviations is summarised in *Appendix I.*

6.Conclusion and future work

A rapid and computationally less expensive approach for the automatic identification of lung adenocarcinoma has been proposed in this paper. The method is based on a lightweight neural network framework that achieves encouraging correctness when we match it with any other existing procedures. The model may be used to detect adenocarcinoma using Lung 2D-CT scans with 100% accuracy by training it on the benchmark LIDC-IDRI dataset, which has a distribution like the data on which the predictions are to be made.

In the future, the proposed model could be trained using a larger dataset including other imaging modalities such as X-ray or PET scans of people belonging to different geographical locations and age groups. The segmentation procedure could also be employed in subsequent research, by evaluating parameters such as slice thickness, complexity class, estimated tumour size, and tumour location and assigning a confidence score to each segmented region. The proposed approach could also be tested in a prospective clinical trial setting for evaluating tumour response to treatment using the automatic volumetric measurement. The management of lung cancer patients could highly benefit from the clinical implementation of this detection model after prospective validation as it offers a quick and accurate diagnosis. Additionally, the model's usage in extensive radiomics research will enable automation and shorten the detection time. Given the challenge of obtaining large labelled datasets, techniques that allow models to learn from small datasets or leverage knowledge from related tasks will be of great interest. Advances in neural network-based lung cancer detection, like all medical technologies, must be pursued with a patient-centric approach to ensure that the technology improves care quality, accessibility, and results.

Acknowledgment

None.

Conflicts of interest

The authors have no conflicts of interest to declare.

Data availability

The LIDC-IDRI dataset is publicly accessible at https://wiki.cancerimagingarchive.net/plugins/servlet/mobile?contentId=1966254#content/view/1966254.

Author's contribution statement

Manika Jha: Conceptualization, Data collection, Writing – original draft, Writing – editing. **Richa Gupta:** Analysis and Interpretation of results. **Rajiv Saxena:** Investigation on challenges and Final Supervision.

References

[1] Cokkinides V, Albano J, Samuels A, Ward M, Thum J. American cancer society: cancer facts and figures. Atlanta: American Cancer Society. 2005.

[2] https://www.who.int/news-room/fact-sheets/detail/cancer. Accessed 02 December 2023.
[3] https://www.curetoday.com/view/world-lung-cancer-day-2019-facts--figures. Accessed 02 December 2023.
[4] Jha M, Gupta R, Saxena R. A framework for in-vivo human brain tumor detection using image augmentation and hybrid features. Health Information Science and Systems. 2022; 10(1):23.
[5] Liu Z, Wang J, Yuan Z, Zhang B, Gong L, Zhao L, et al. Preliminary results about application of intensity-modulated radiotherapy to reduce prophylactic radiation dose in limited-stage small cell lung cancer. Journal of Cancer. 2018; 9(15):2625-30.
[6] Elizabeth JV, Aslam SM. An intelligent disease prediction and monitoring system using feature selection, multi-neural network and fuzzy rules. Neural Computing and Applications. 2022; 34(22):19877-93.
[7] Zou G, Fu G, Han B, Wang W, Liu C. Series arc fault detection based on dual filtering feature selection and improved hierarchical clustering sensitive component selection. IEEE Sensors Journal. 2023; 23(6):6050-60.
[8] Gambino O, Conti V, Galdino S, Valenti CF, Dos SWP. Image segmentation techniques for healthcare systems. Journal of Healthcare Engineering. 2019; 2019:1-3.
[9] Liu D, Brace CL. CT imaging during microwave ablation: analysis of spatial and temporal tissue contraction. Medical Physics. 2014; 41(11):113303.
[10] Jha M, Gupta R, Saxena R. A review on non-invasive biosensors for early detection of lung cancer. In 6th international conference on signal processing and communication 2020 (pp. 162-6). IEEE.
[11] Chabat F, Yang GZ, Hansell DM. Obstructive lung diseases: texture classification for differentiation at CT. Radiology. 2003; 228(3):871-7.
[12] Zhu Y, Tan Y, Hua Y, Wang M, Zhang G, Zhang J. Feature selection and performance evaluation of support vector machine (SVM)-based classifier for differentiating benign and malignant pulmonary nodules by computed tomography. Journal of Digital Imaging. 2010; 23:51-65.
[13] Kadir T, Gleeson F. Lung cancer prediction using machine learning and advanced imaging techniques. Translational Lung Cancer Research. 2018; 7(3):304-12.
[14] Makaju S, Prasad PW, Alsadoon A, Singh AK, Elchouemi A. Lung cancer detection using CT scan images. Procedia Computer Science. 2018; 125:107-14.
[15] Dev C, Kumar K, Palathil A, Anjali T, Panicker V. Machine learning based approach for detection of lung cancer in DICOM CT image. In ambient communications and computer systems: RACCCS 2019 (pp. 161-73). Springer Singapore.
[16] Hussain L, Aziz W, Alshdadi AA, Nadeem MS, Khan IR. Analyzing the dynamics of lung cancer imaging data using refined fuzzy entropy methods by extracting different features. IEEE Access. 2019; 7:64704-21.
[17] Talukder MA, Islam MM, Uddin MA, Akhter A, Hasan KF, Moni MA. Machine learning-based lung and colon cancer detection using deep feature extraction and ensemble learning. Expert Systems with Applications. 2022; 205:117695.
[18] Hussain L, Almaraashi MS, Aziz W, Habib N, Saif ASU. Machine learning-based lungs cancer detection using reconstruction independent component analysis and sparse filter features. Waves in Random and Complex Media. 2021:1-26.
[19] Razmjooy N, Ashourian M, Karimifard M, Estrela VV, Loschi HJ, Do ND, et al. Computer-aided diagnosis of skin cancer: a review. Current Medical Imaging. 2020; 16(7):781-93.
[20] Lakshmanaprabu SK, Mohanty SN, Shankar K, Arunkumar N, Ramirez G. Optimal deep learning model for classification of lung cancer on CT images. Future Generation Computer Systems. 2019; 92:374-82.
[21] Wang X, Chen H, Gan C, Lin H, Dou Q, Tsougenis E, et al. Weakly supervised deep learning for whole slide lung cancer image analysis. IEEE Transactions on Cybernetics. 2019; 50(9):3950-62.
[22] Zhou Y, Lu Y, Pei Z. Accurate diagnosis of early lung cancer based on the convolutional neural network model of the embedded medical system. Microprocessors and Microsystems. 2021; 81:103754.
[23] Shakeel PM, Burhanuddin MA, Desa MI. Automatic lung cancer detection from CT image using improved deep neural network and ensemble classifier. Neural Computing and Applications. 2022:1-4.
[24] Aggarwal T, Furqan A, Kalra K. Feature extraction and LDA based classification of lung nodules in chest CT scan images. In international conference on advances in computing, communications and informatics 2015 (pp. 1189-93). IEEE.
[25] Deepa P, Suganthi M. A fuzzy shape representation of a segmented vessel tree and kernel-induced random forest classifier for the efficient prediction of lung cancer. The Journal of Supercomputing. 2020; 76(8):5801-24.
[26] Hoque A, Farabi AA, Ahmed F, Islam MZ. Automated detection of lung cancer using CT scan images. In region 10 symposium 2020 (pp. 1030-3). IEEE.
[27] Mathews AB, Jeyakumar MK. Automatic detection of segmentation and advanced classification algorithm. In fourth international conference on computing methodologies and communication 2020 (pp. 358-62). IEEE.
[28] Ozdemir O, Russell RL, Berlin AA. A 3D probabilistic deep learning system for detection and diagnosis of lung cancer using low-dose CT scans. IEEE Transactions on Medical Imaging. 2019; 39(5):1419-29.
[29] Ali I, Muzammil M, Haq IU, Khaliq AA, Abdullah S. Efficient lung nodule classification using transferable texture convolutional neural network. IEEE Access. 2020; 8:175859-70.

[30] Kareem HF, AL-husieny MS, Mohsen FY, Khalil EA, Hassan ZS. Evaluation of SVM performance in the detection of lung cancer in marked CT scan dataset. Indonesian Journal of Electrical Engineering and Computer Science. 2021; 21(3):1731-8.

[31] Sori WJ, Feng J, Godana AW, Liu S, Gelmecha DJ. DFD-Net: lung cancer detection from denoised CT scan image using deep learning. Frontiers of Computer Science. 2021; 15:1-3.

[32] Priya MM, Jawhar SJ, Geisa JM. Optimal deep belief network with opposition based pity beetle algorithm for lung cancer classification: a DBNOPBA approach. Computer Methods and Programs in Biomedicine. 2021; 199:105902.

[33] Neal JES, Bhattacharyya D, Chakkravarthy M, Byun YC. 3D CNN with visual insights for early detection of lung cancer using gradient-weighted class activation. Journal of Healthcare Engineering. 2021; 2021:1-11.

[34] Asuntha A, Srinivasan A. Deep learning for lung cancer detection and classification. Multimedia Tools and Applications. 2020; 79:7731-62.

[35] Ramana K, Kumar MR, Sreenivasulu K, Gadekallu TR, Bhatia S, Agarwal P, et al. Early prediction of lung cancers using deep saliency capsule and pre-trained deep learning frameworks. Frontiers in Oncology. 2022; 12:886739.

[36] Causey JL, Li K, Chen X, Dong W, Walker K, Qualls JA, et al. Spatial pyramid pooling with 3D convolution improves lung cancer detection. IEEE/ACM Transactions on Computational Biology and Bioinformatics. 2020; 19(2):1165-72.

[37] Kumar V, Altahan BR, Rasheed T, Singh P, Soni D, Alsaab HO, et al. Improved UNet deep learning model for automatic detection of lung cancer nodules. Computational Intelligence and Neuroscience. 2023; 2023:1-8.

[38] Tiwari L, Raja R, Sharma V, Miri R. Fuzzy inference system for efficient lung cancer detection. In computer vision and machine intelligence in medical image analysis: international symposium 2019 (pp. 33-41). Springer Singapore.

[39] Armato IIISG, Mclennan G, Bidaut L, Mcnitt-gray MF, Meyer CR, Reeves AP, et al. The lung image database consortium (LIDC) and image database resource initiative (IDRI): a completed reference database of lung nodules on CT scans. Medical Physics. 2011; 38(2):915-31.

[40] Zeinali Y, Niaki ST. Heart sound classification using signal processing and machine learning algorithms. Machine Learning with Applications. 2022; 7:100206.

[41] Fallahi A, Pooyan M, Lotfi N, Baniasad F, Tapak L, Mohammadi-mobarakeh N, et al. Dynamic functional connectivity in temporal lobe epilepsy: a graph theoretical and machine learning approach. Neurological Sciences. 2021; 42:2379-90.

[42] Janghel RR, Verma A, Rathore YK. Performance comparison of machine learning techniques for epilepsy classification and detection in EEG signal. In data management, analytics and innovation: proceedings of ICDMAI, 2020 (pp. 425-38). Springer Singapore.

[43] Hisham S, Makhtar M, Aziz AA. Anomaly detection in smart contracts based on optimal relevance hybrid features analysis in the ethereum blockchain employing ensemble learning. International Journal of Advanced Technology and Engineering Exploration. 2023; 10(109):152-79.

[44] Ignatious S, Joseph R. Computer aided lung cancer detection system. In global conference on communication technologies 2015 (pp. 555-8). IEEE.

[45] Srinath R, Gayathri R. Detection and classification of electroencephalogram signals for epilepsy disease using machine learning methods. International Journal of Imaging Systems and Technology. 2021; 31(2):729-40.

[46] Kumar DM, Satyanarayana D, Prasad MG. MRI brain tumor detection using optimal possibilistic fuzzy C-means clustering algorithm and adaptive k-nearest neighbor classifier. Journal of Ambient Intelligence and Humanized Computing. 2021; 12(2):2867-80.

[47] Liu S, Shan T, Tao R, Zhang YD, Zhang G, Zhang F, et al. Sparse discrete fractional fourier transform and its applications. IEEE Transactions on Signal Processing. 2014; 62(24):6582-95.

[48] Battineni G, Chintalapudi N, Amenta F, Traini E. A comprehensive machine-learning model applied to magnetic resonance imaging (MRI) to predict alzheimer's disease (AD) in older subjects. Journal of Clinical Medicine. 2020; 9(7):2146.

[49] Świetlik D, Białowąs J. Application of artificial neural networks to identify alzheimer's disease using cerebral perfusion SPECT data. International Journal of Environmental Research and Public Health. 2019; 16(7):1303.

[50] Veena A, Gowrishankar S. Context based healthcare informatics system to detect gallstones using deep learning methods. International Journal of Advanced Technology and Engineering Exploration. 2022; 9(96):1661-77.

[51] Nemade V, Pathak S, Dubey AK. A systematic literature review of breast cancer diagnosis using machine intelligence techniques. Archives of Computational Methods in Engineering. 2022; 29(6):4401-30.

[52] Webber JW, Elias K. Multi-cancer classification; an analysis of neural network models. Machine Learning with Applications. 2023; 12:100468.

[53] Masood A, Yang P, Sheng B, Li H, Li P, Qin J, et al. Cloud-based automated clinical decision support system for detection and diagnosis of lung cancer in chest CT. IEEE Journal of Translational Engineering in Health and Medicine. 2019; 8:1-3.

Manika Jha received her B.Tech. degree in Instrumentation and Control Engineering from Guru Gobind Singh Indraprastha University, New Delhi, India in 2016 and M.Tech. degree in Robotics and automation from Indira Gandhi Delhi Technical University, New Delhi, India in 2019. She is currently pursuing the Ph.D. degree Electronics and Communication Engineering Department at Jaypee Institute of Information Technology, Noida, India. Her research interests include Biomedical Signal Processing, Machine Learning, Deep Learning, Natural Language Processing, Medical Image Processing, and Genomic Signal Processing.
Email: Jhamanika1994@gmail.com

Richa Gupta has done her Ph.D. from JIIT, Noida, India in Joint Source Channel coding in 2013, M.Tech. from IIT Kanpur, India in Information Systems in 2005 and B.Tech. in Electronics and Communication Engineering branch from KIET, Ghaziabad, India in 2003. She is currently holding the post of Associate Professor in the department of ECE department at JIIT Noida. Her research area includes Machine Learning, Image Processing and Multimedia Signal Processing.
Email: richa.gupta@jiit.ac.in

Rajiv Saxena obtained B.E. in Electronics and Telecommunication Engineering and M.E. in Digital Techniques and Data Processing. He joined IIT, Roorkee (erstwhile UOR, Roorkee), as a QIP Research Fellow, towards his Doctoral Degree Program. The Ph. D. degree was conferred on him in Electronics and Computer Engineering. He has supervised Twenty Ph.D. candidates in Wireless, Cellular, Mobile and Digital Communication, Digital Signal Processing, Digital Image Processing, and Application of DSP tools in Electronic Systems and Bio-Medical Engineering. He has published about 100 research articles in refereed journals of national and international repute.
Email: srajiv2008@gmail.com

Appendix I

S. No.	Abbreviation	Description
1	2D-CT	Two-Dimensional Computed Tomography
2	2D-FrFT	Two-Dimensional Fractional Fourier Transform
3	3DDCNN	Three-Dimensional Deep Convolutional Neural Network
4	AUC	Area Under Curve
5	AUROC	Area Under Receiver Operating Characteristic
6	CAD	Computer Aided Diagnostic
7	CNN	Convolutional Neural Network
8	CT	Computed Tomography
9	DL	Deep Learning
10	DNN	Deep Neural Network
11	FCN	Fully Convolutional Network
12	FPSO	Fuzzy Particle Swarm Optimization
13	GLCM	Grey Level Co-Occurrence Matrix
14	HOG	Histogram of Gradient
15	LBP	Local Binary Pattern
16	LIDC-IDRI	Lung Image Database Consortium Image Collection
17	MFE	Multiscale Fuzzy Entropy
18	MMSE	Minimum Mean Square Error
19	MPE	Multiscale Permutation Entropy
20	MSE	Multiscale Sample Entropy
21	NED	Neural Ensemble-based Detection
22	NSCLC	Non-Small Cell Lung Cancer
23	PET	Position Emission Tomography
24	PSNR	Peak Signal to Noise Ratio
25	RCMFE	Refined Composite Multiscale Fuzzy Entropy
26	RNN	Recurrent Neural Networks
27	ROC	Receiver Operating Characteristic
28	mRPN	Region Proposal Network
29	SGLDM	Spatial Grey Level Dependence Matrix
30	SVM	Support Vector Machine